Biophysical Journal, Volume *114*

Supplemental Information

Atomistic Scale Effects of Lipopolysaccharide Modifications on Bacterial Outer Membrane Defenses

Amy Rice and Jeff Wereszczynski

S1 Comparison of Symmetric and Asymmetric Bilayers

S1.1 System preparation

To determine whether the opposing leaflet affected properties of the LPS monolayer, two asymmetric bilayers consisting of either pure LPS or mLPS in one leaflet and pure POPE in the opposing leaflet were constructed. Final coordinates from the LPS bilayer simulation were used as starting coordinates for the LPS leaflet, while a POPE leaflet containing 109 lipids and the appropriate x-y dimensions was constructed using the CHARMM-GUI membrane builder [1, 2]. The two leaflets were aligned by hand, then neutralizing Ca^{2+} ions were added to the core region of the LPS leaflet and 20 Å water with 0.15 M NaCl was added in the ± z dimensions. The asymmetric mLPS/POPE was constructed in a similar manner, with the POPE leaflet containing 119 lipids to accommodate the increased lipid area of mLPS. The C36 lipid [3, 4] parameter set was used for POPE. Minimization, heating, and water equilibration were performed as described above, followed by 1000 ns of long time-scale equilibration prior to simulation on Anton 2 [5]. Both systems were simulated on Anton 2 for 7.0 µs each, with the first 2.0 µs removed as equilibration.

S1.2 Comparison of bilayer properties

No differences were observed in the hydrophobic thickness of the leaflets, though slight differences in the area per lipid were observed (Figure S1 and Table S1); these modest changes in area could be due to a slight area mismatch between the two leaflets. A related small increase in tail ordering was also observed in the LPS/POPE system (Figure S2), while a slight decrease was observed in the mLPS/POPE system; we note that the differences here are much smaller than those present between LPS types with or without palmitoylation (Figure 5). Density profiles of all four systems along the bilayer normal (Figure S3) reveal that the location of key moieties, such as the acyl tails, phosphate groups, calcium ions, and water, were largely unchanged between systems with and without POPE. The similarities displayed in Ca^{2+} coordination (Table S2) substantiate this result. Finally, no significant differences between inter-lipid A or inter-LPS binding were observed (Table S3).

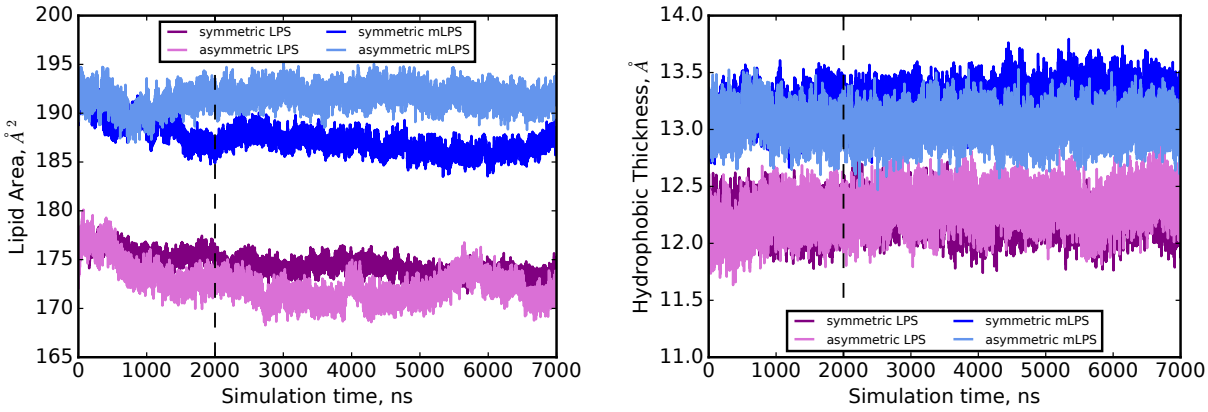

Figure S1: Area per lipid (left) and hydrophobic thickness (right) for symmetric LPS (purple), the LPS leaflet of the LPS/POPE bilayer (pink), symmetric mLPS (blue), and the mLPS leaflet of the mLPS/POPE bilayer (light blue). The dashed horizontal line at 2.0 µs indicates the portion of the trajectory that was removed as equilibration.

System	Lipid Area (Å^2)	Hydrophobic Thickness, per leaflet (Å)	Area per lipid tail (Å^2)
symmetric LPS	174.0 ± 0.3	12.2 ± 0.1	29.0 ± 0.1
asymmetric LPS- LPS leaflet	171.8 ± 0.4	12.3 ± 0.1	28.6 ± 0.1
symmetric mLPS	186.8 ± 0.2	13.3 ± 0.1	26.7 ± 0.1
asymmetric mLPS- mLPS leaflet	191.8 ± 0.1	13.1 ± 0.1	27.4 ± 0.1
asymmetric LPS- POPE leaflet	56.7 ± 0.1	18.9 ± 0.1	28.4 ± 0.1
asymmetric mLPS- POPE leaflet	58.0 ± 0.1	18.6 ± 0.1	29.0 ± 0.1

Table S1: Mesoscopic bilayer properties for the symmetric LPS, LPS/POPE, symmetric mLPS, and mLPS/POPE bilayer systems.

System	Ca^{2+}–Wat	Ca^{2+}– P_{LipA}	Ca^{2+}– P_{Core}	Ca^{2+}– C_{core}
symmetric LPS	3.5	1.0	1.0	0.2
asymmetric LPS	3.4	1.0	1.0	0.2
symmetric mLPS	3.6	0.6	1.3	0.3
asymmetric mLPS	3.5	0.6	1.3	0.3

Table S2: Coordination numbers for Ca^{2+} in the symmetric and asymmetric LPS and mLPS bilayer systems, corresponding to the integration up through the first peak of the respective radial distribution functions. P_{LipA} and P_{Core} correspond to the phosphorus atoms in the lipid A head group and in the core oligosaccharide region, respectively; C_{core} corresponds to the carboxyl carbons in the inner core.

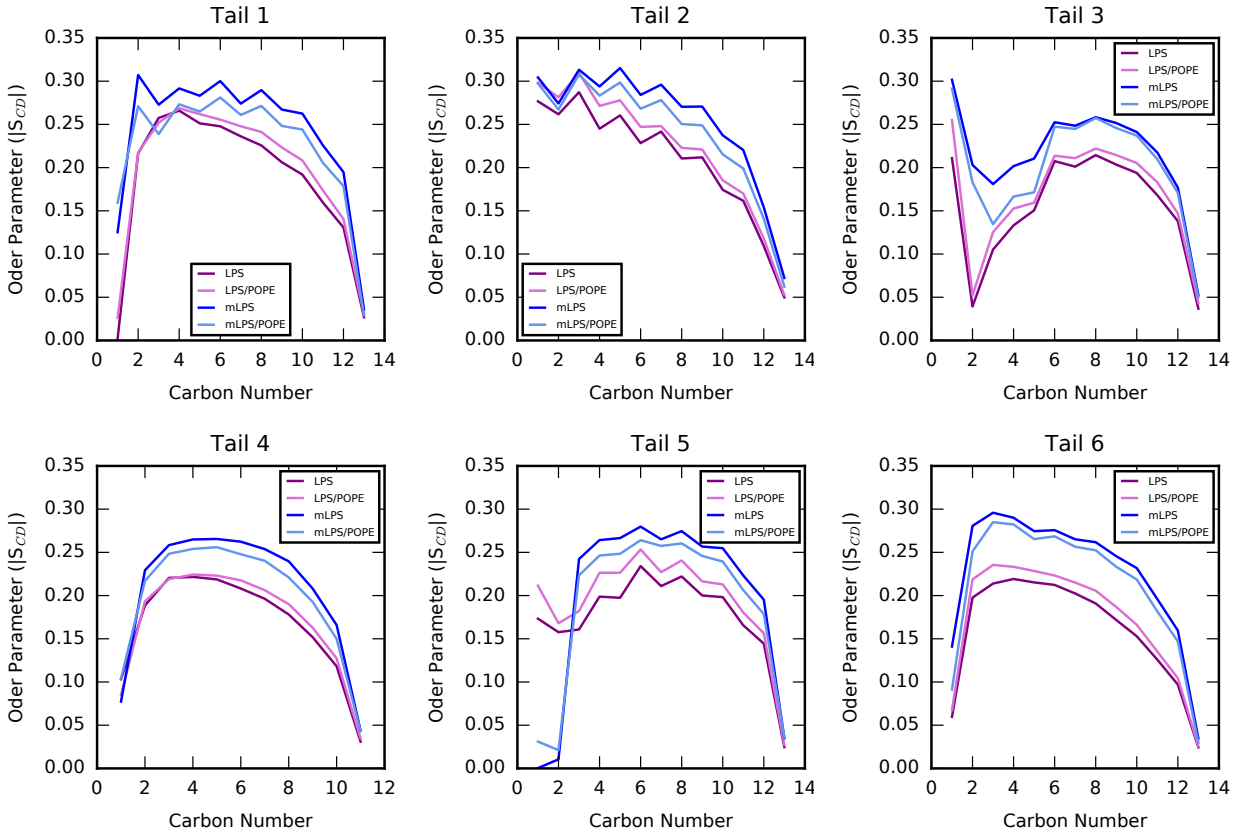

Figure S2: Lipid tail order parameters ($|S_{cd}|$) for all six lipid tails. Data for the symmetric and asymmetric LPS bilayer leaflets are shown in purple and pink, respectively, while data for the symmetric and asymmetric mLPS bilayer leaflets are shown in shades of blue.

System	Inter-LPS Hydrogen Bonds	Inter-lipid A Hydrogen Bonds
symmetric LPS	2.83 ± 0.06	0.75 ± 0.02
asymmetric LPS	2.81 ± 0.01	0.71 ± 0.01
symmetric mLPS	4.29 ± 0.04	2.34 ± 0.02
asymmetric mLPS	4.35 ± 0.03	2.40 ± 0.02

Table S3: Inter-LPS and inter-lipid A hydrogen bonding for the symmetric and asymmetric LPS and mLPS bilayer systems.

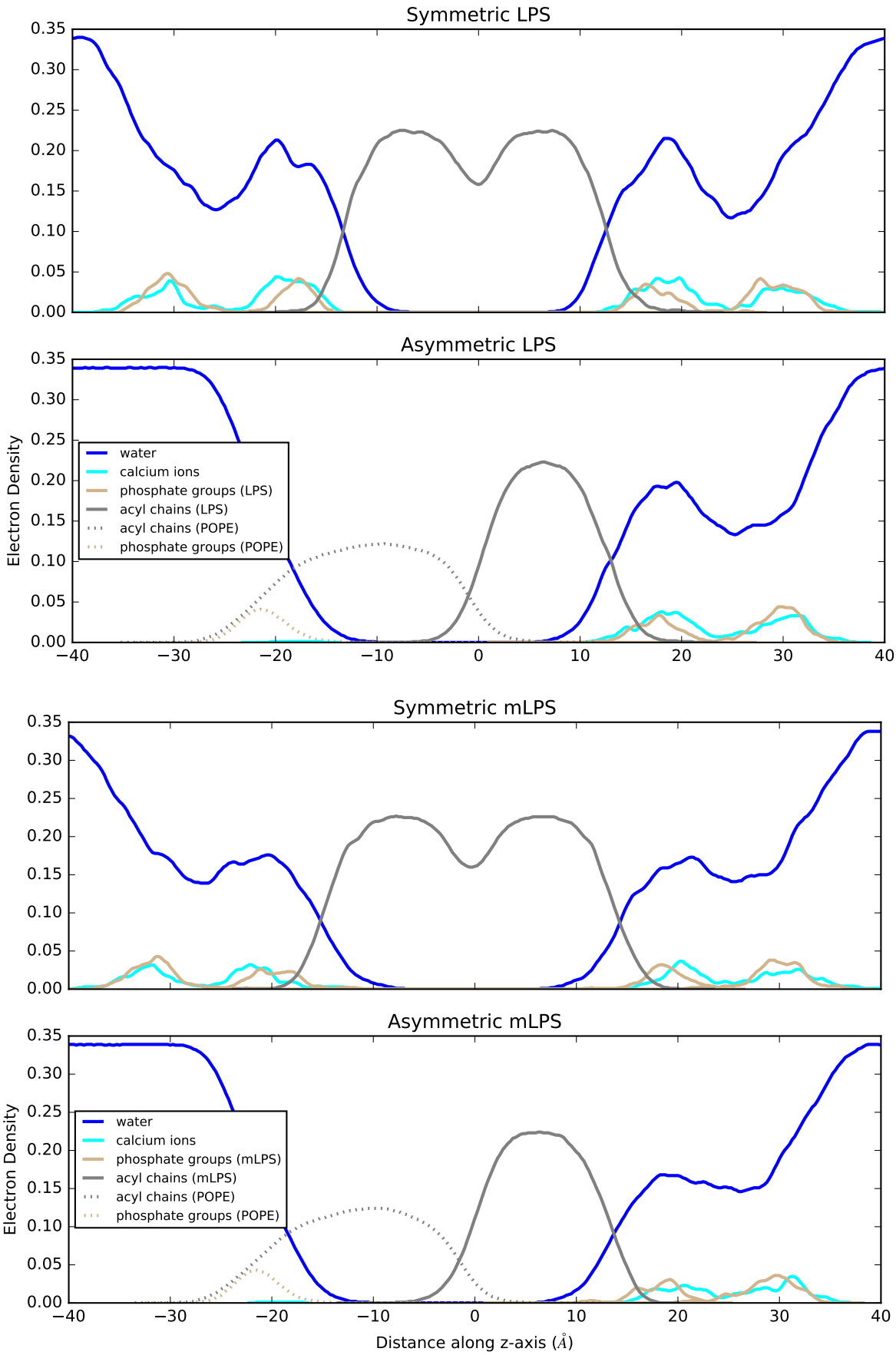

Figure S3: Density profiles along the bilayer normal for the symmetric LPS, asymmetric LPS/POPE, symmetric mLPS, and asymmetric mLPS/POPE bilayers.

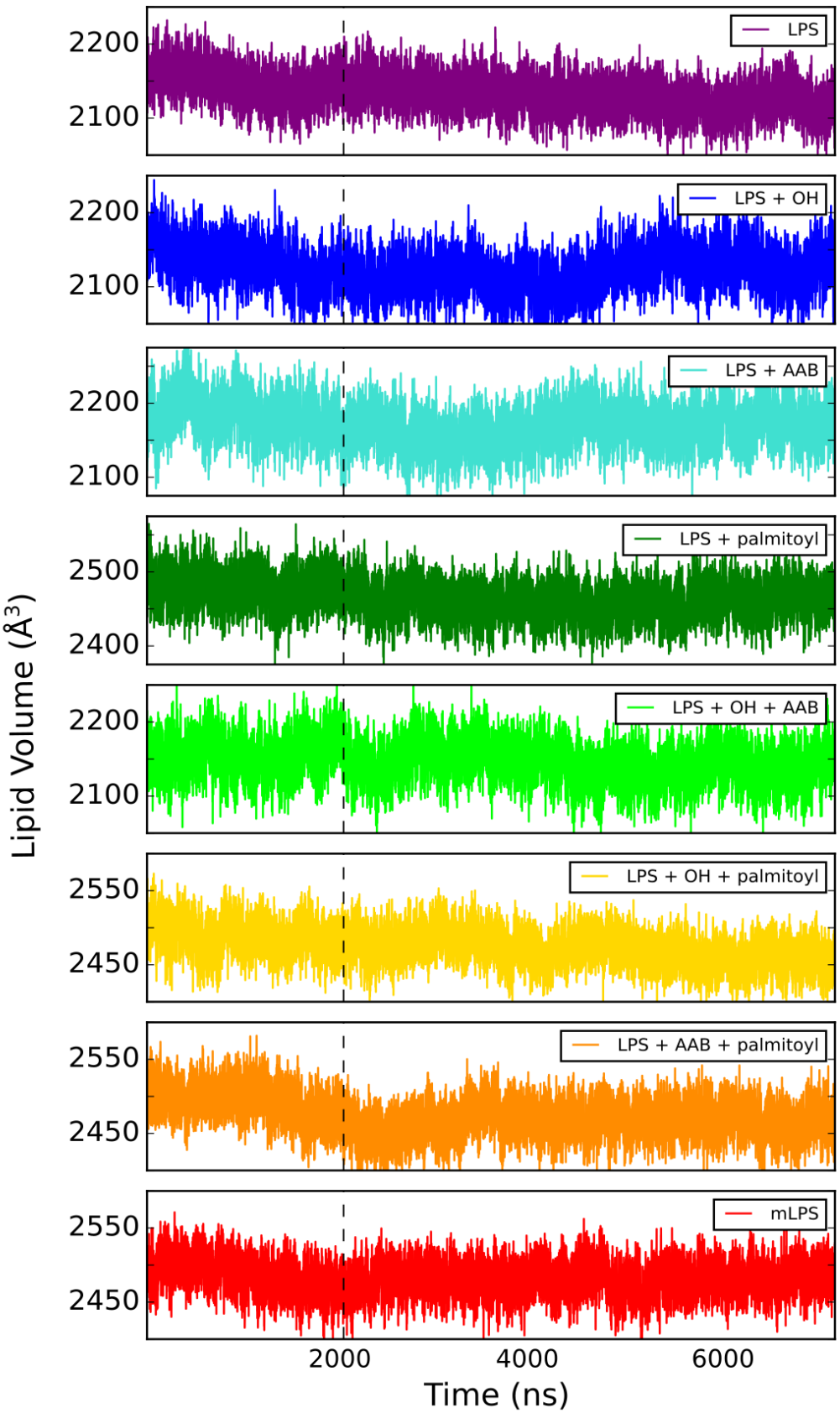

Figure S4: Average lipid volume for all eight systems over the full 7.0 µs. The dashed horizontal line at 2.0 µs indicates the portion of the trajectory that was removed as equilibration.

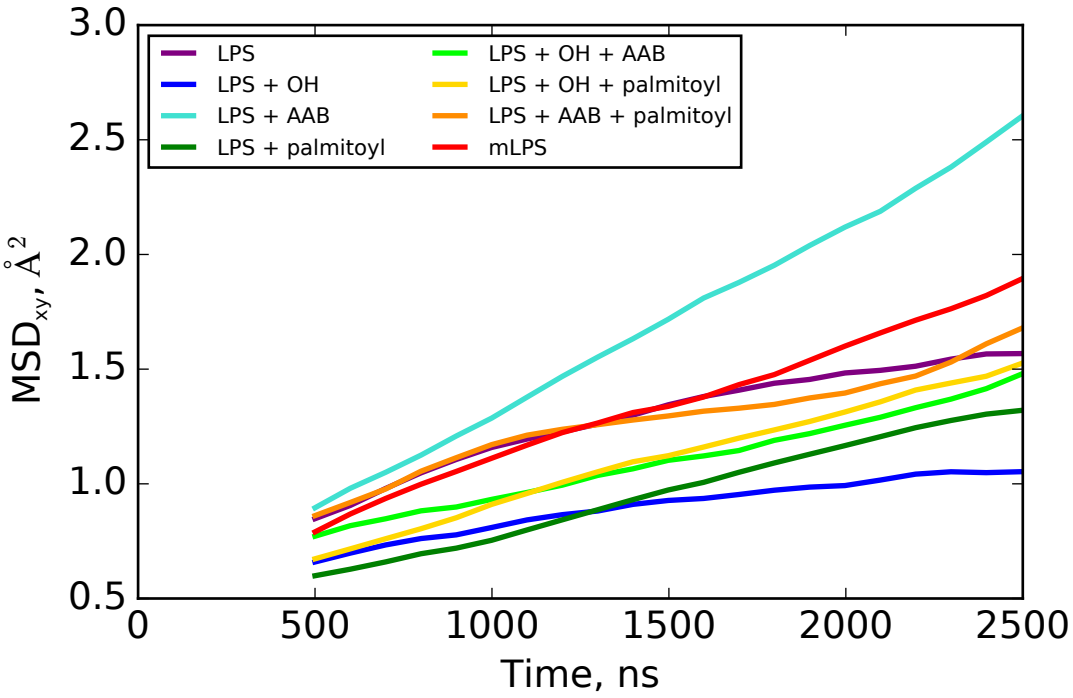

Figure S5: Plots of MSD in the xy-plane versus time for all eight bilayer systems.

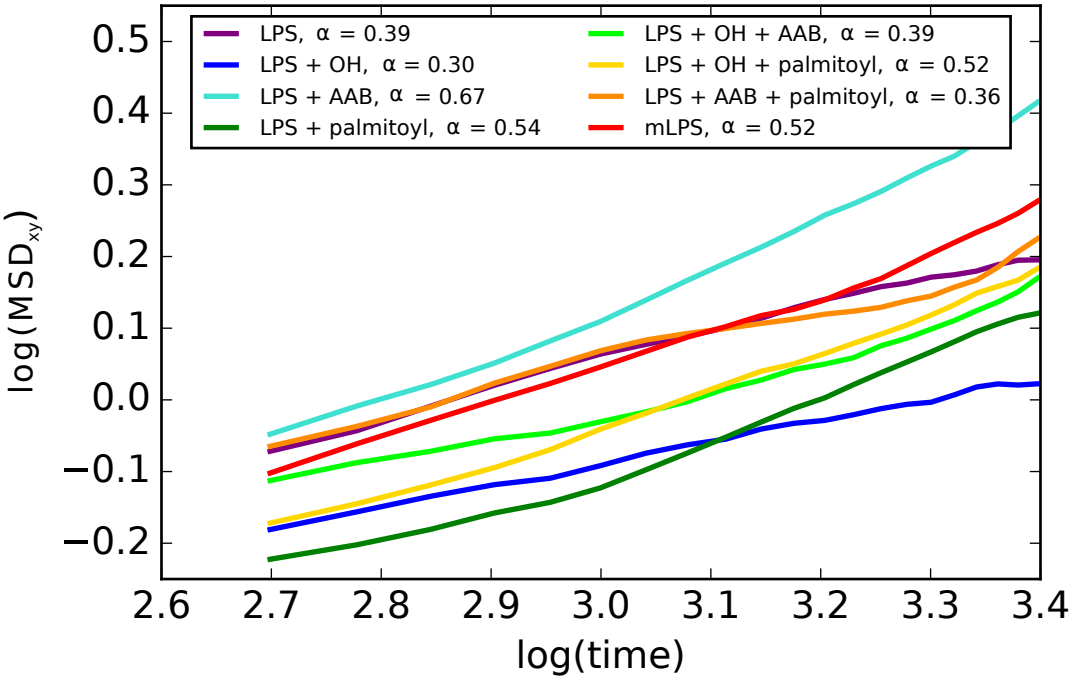

Figure S6: Data from Figure S5 on a log-log plot, highlighting the subdiffusive nature. Diffusion processes follow the power law MSD $\sim Dt^{\alpha}$. In typical diffusion, $\alpha = 1$, while cases with $\alpha < 1$ are subdiffusive. Here, the slope of the best fit line is given for each system, corresponding to α.

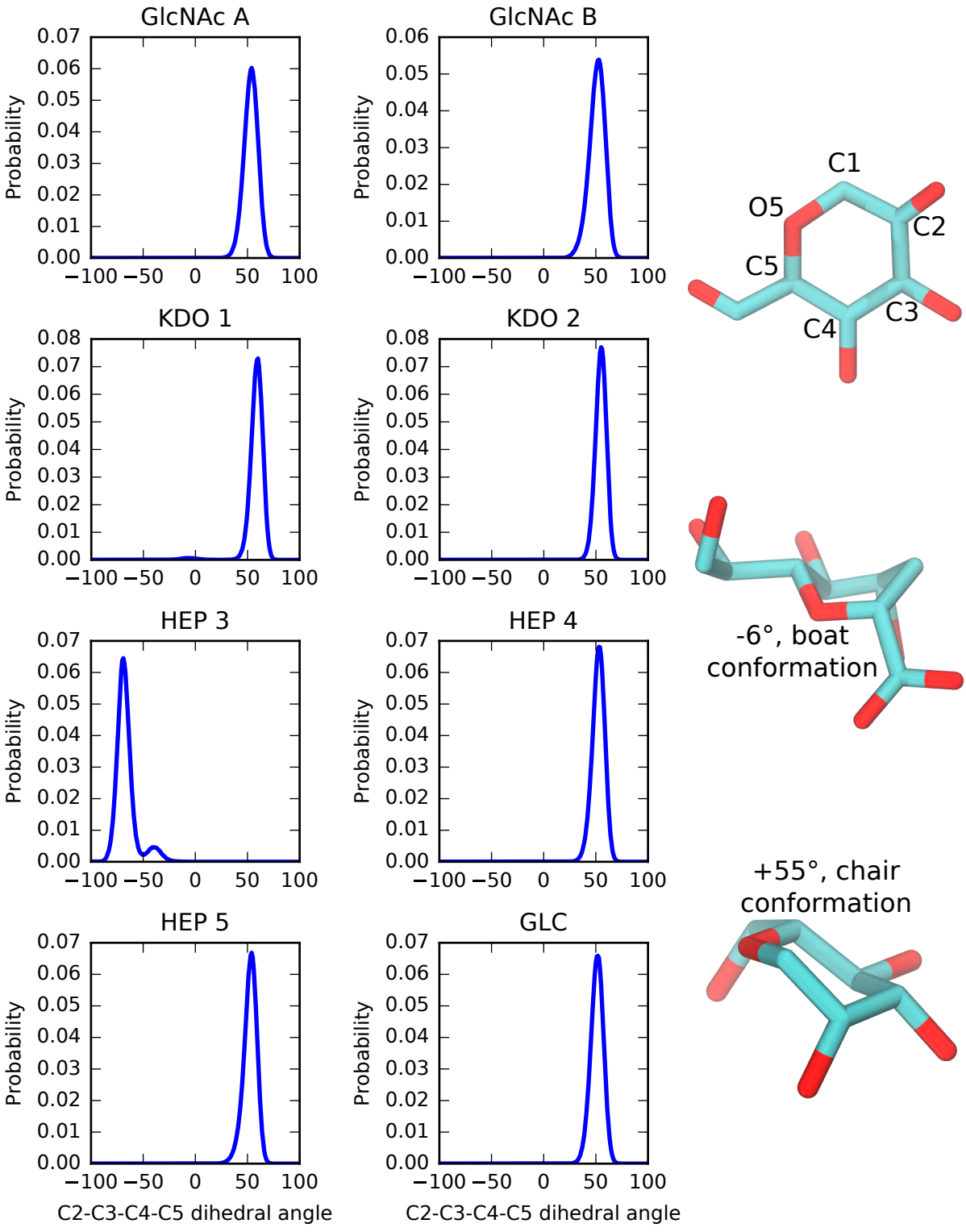

Figure S7: C2–C3–C4–C5 dihedral angles for all eight pyranoses. Values near ±55 represent the two possible chair conformations, while values closer to 0 represent boat and twist-boat conformations.

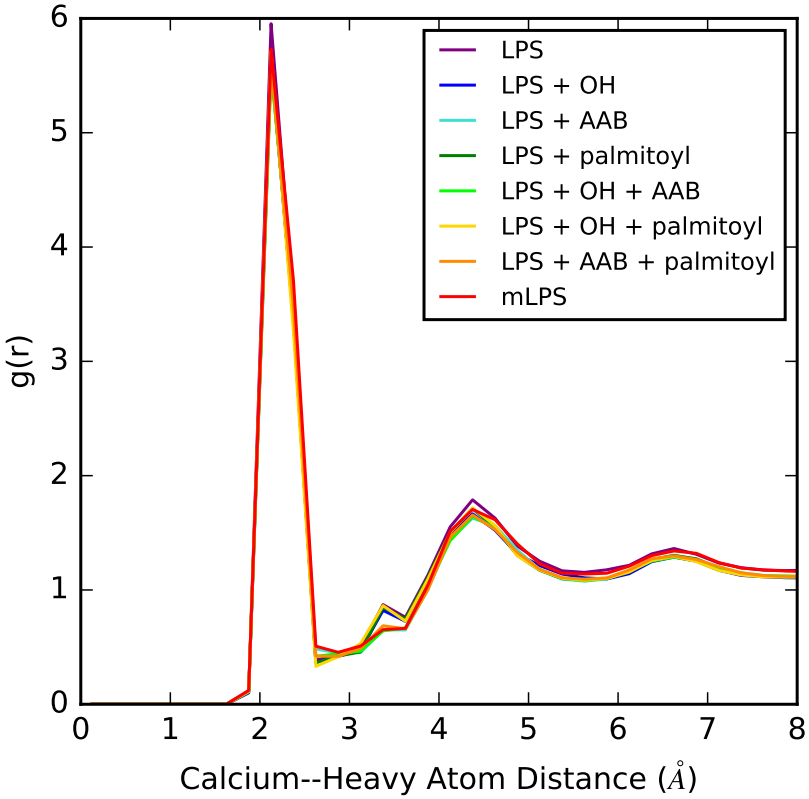

Figure S8: Calcium–heavy atom radial distribution functions (RDFs) for all eight systems. Integration of the first peak, up through 2.5 Å yields a coordination number of 6 for all systems.

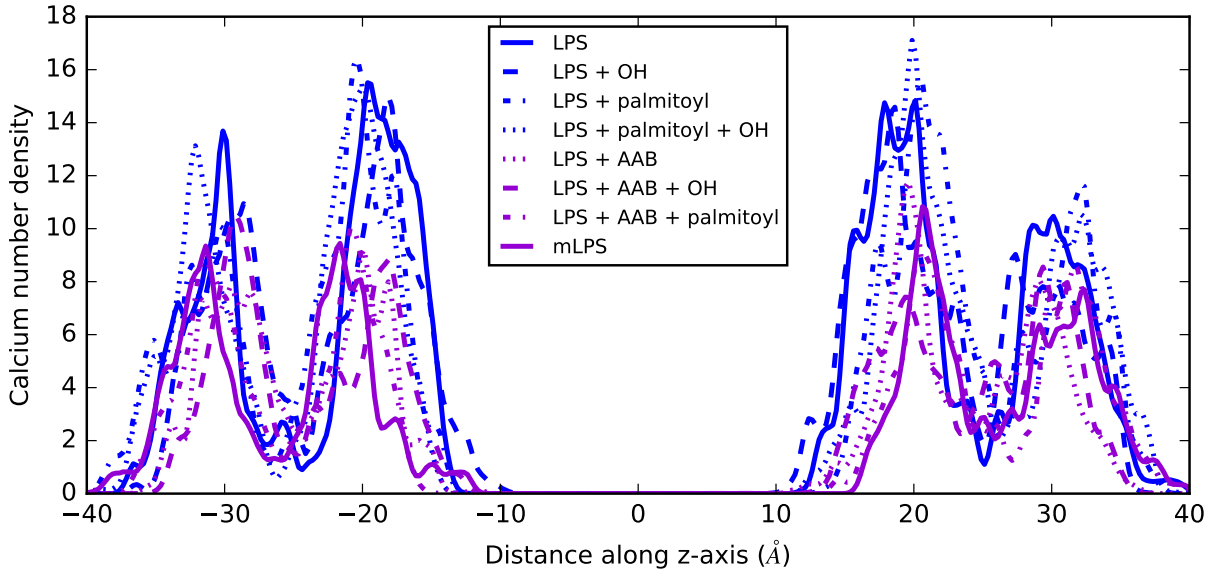

Figure S9: Calcium number density along the bilayer normal for all eight systems. The presence of aminoarabinose leads to a decreased density of calcium around the lipid A phosphate groups.

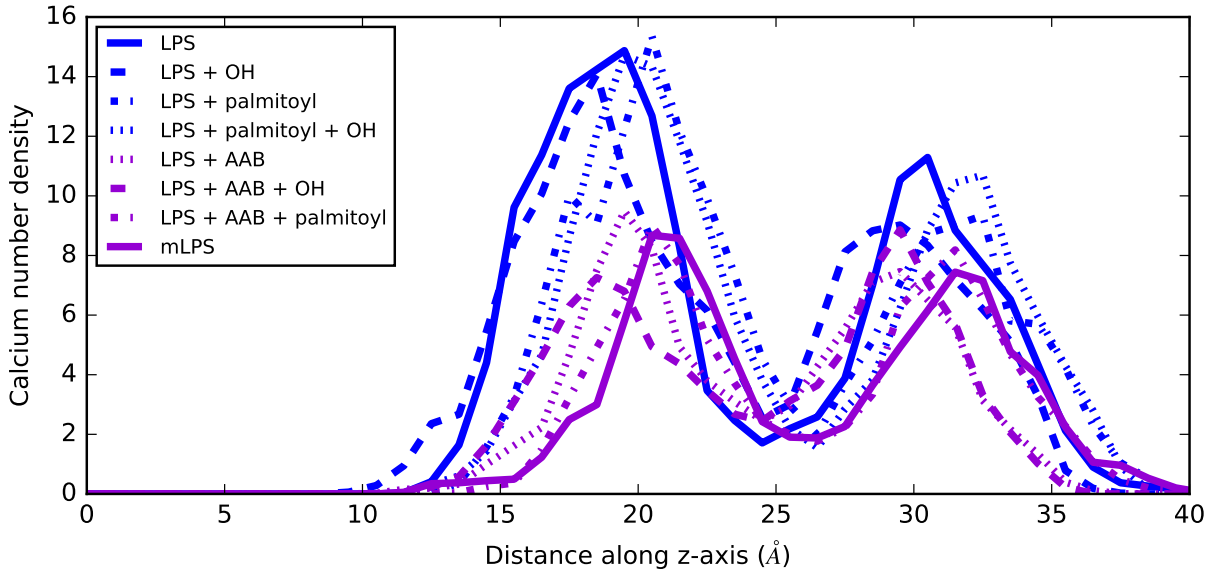

Figure S10: Symmetric calcium number density along the bilayer normal for all eight systems. The presence of aminoarabinose leads to a decreased density of calcium around the lipid A phosphate groups.

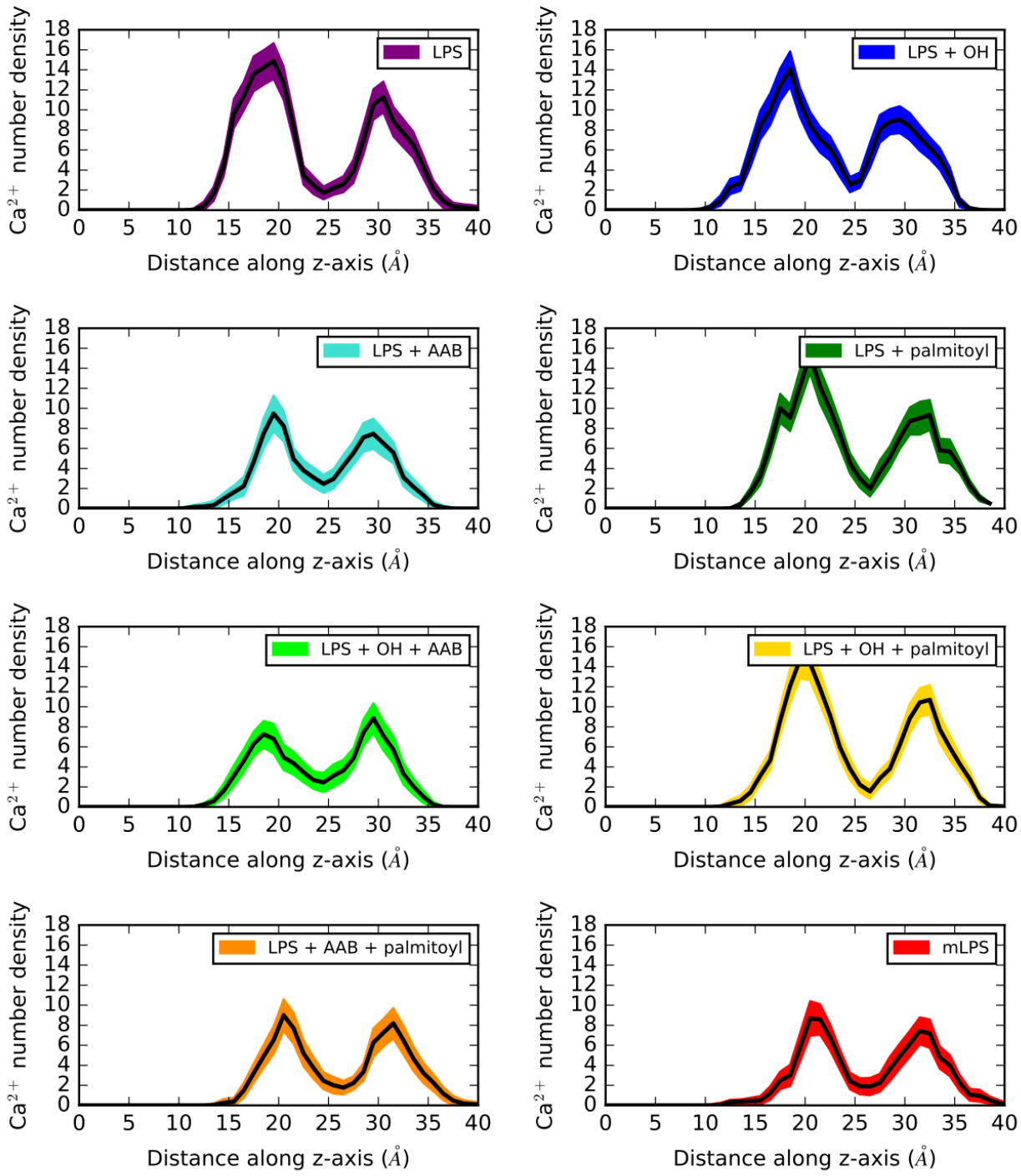

Figure S11: Symmetric calcium number density along the bilayer normal for all eight systems, with standard deviations indicated by the colored regions.

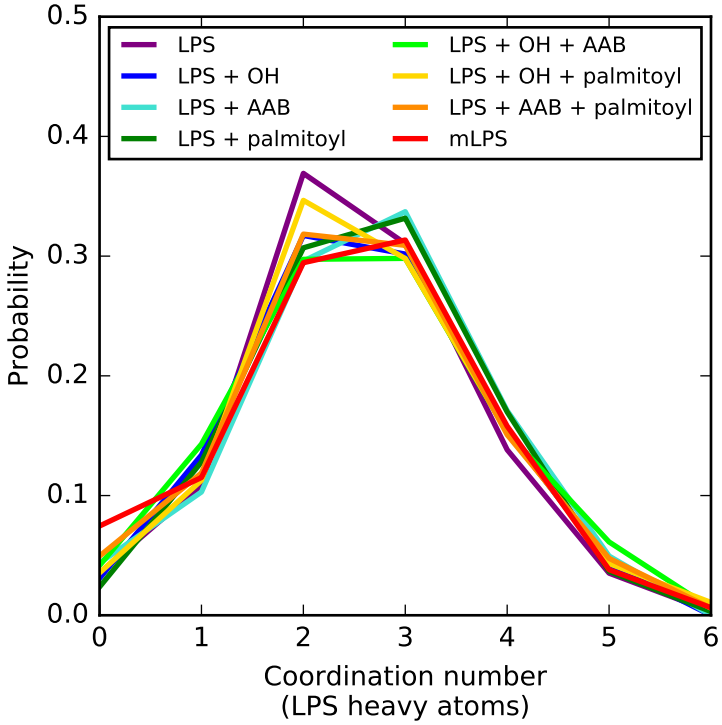

Figure S12: Probability distribution of calcium–LPS heavy atom coordination number for all eight systems.

System	LIPA:PA	LIPA:C=O (inter)	LIPA:C=O (intra)	KDO2:COO
LPS + AAB	0.7	0.3	0.1	0.1
LPS + OH + AAB	0.7	0.3	0.2	0.1
LPS + AAB + palmitoyl	0.7	0.4	0.2	0.1
mLPS	0.7	0.3	0.2	0.1

Table S4: Aminoarabinose probability of hydrogen bonding with different moieties for all four systems that contain aminoarabinose. Only the dominant hydrogen bond acceptors ($P \geq 0.1$) are listed.

System	LIPA:P_A – LIPA:P_B	HEP3:P – HEP5:P (inter)	HEP3:P HEP5:P (intra)	LIPA:P_A– KDO2:COO	LIPA:P_B – KDO1:COO
LPS	0.4	0.3	0.3	0.1	0.1
LPS + OH	0.4	0.2	0.2	0.1	0.1
LPS + AAB	0.1	0.3	0.3	0.2	0.0
LPS + palmitoyl	0.3	0.2	0.2	0.1	0.1
LPS + OH + AAB	0.1	0.4	0.4	0.2	0.0
LPS + OH + palmitoyl	0.4	0.3	0.3	0.1	0.1
LPS + AAB + palmitoyl	0.1	0.3	0.3	0.3	0.0
mLPS	0.1	0.4	0.4	0.3	0.0

Table S5: Calcium-mediated interactions for all eight systems. Values listed are the probability that a calcium is bridging these groups; only the dominant bridging interactions ($P \geq 0.1$) are listed.

References

[1] S. Jo, T. Kim, and W. Im. Automated builder and database of protein/membrane complexes for molecular dynamics simulations. *PLoS ONE*, 2(9):e880, 2007.

[2] E. L. Wu, X. Cheng, S. Jo, H. Rui, K. C. Song, E. M. Davila-Contreras, Y. Qi, J. Lee, V. Monje-Galvan, R. M. Venable, J. B. Klauda, and W. Im. CHARMM-GUI Membrane Builder toward realistic biological membrane simulations. *J Comput Chem*, 35(27):1997–2004, Oct 2014.

[3] J. B. Klauda, R. M. Venable, J. A. Freites, J. W. O'Connor, D. J. Tobias, C. Mondragon-Ramirez, I. Vorobyov, A. D. MacKerell, and R. W. Pastor. Update of the CHARMM all-atom additive force field for lipids: validation on six lipid types. *J Phys Chem B*, 114(23):7830–7843, Jun 2010.

[4] R. W. Pastor and A. D. Mackerell. Development of the CHARMM Force Field for Lipids. *J Phys Chem Lett*, 2(13):1526–1532, 2011.

[5] David E. Shaw, J. P. Grossman, Joseph A. Bank, Brannon Batson, J. Adam Butts, Jack C. Chao, Martin M. Deneroff, Ron O. Dror, Amos Even, Christopher H. Fenton, Anthony Forte, Joseph Gagliardo, Gennette Gill, Brian Greskamp, C. Richard Ho, Douglas J. Ierardi, Lev Iserovich, Jeffrey S. Kuskin, Richard H. Larson, Timothy Layman, Li-Siang Lee, Adam K. Lerer, Chester Li, Daniel Killebrew, Kenneth M. Mackenzie, Shark Yeuk-Hai Mok, Mark A. Moraes, Rolf Mueller, Lawrence J. Nociolo, Jon L. Peticolas, Terry Quan, Daniel Ramot, John K. Salmon, Daniele P. Scarpazza, U. Ben Schafer, Naseer Siddique, Christopher W. Snyder, Jochen Spengler, Ping Tak Peter Tang, Michael Theobald, Horia Toma, Brian Towles, Benjamin Vitale, Stanley C. Wang, and Cliff Young. Anton 2: Raising the bar for performance and programmability in a special-purpose molecular dynamics supercomputer. In *Proceedings of the International Conference for High Performance Computing, Networking, Storage and Analysis*, SC '14, pages 41–53, Piscataway, NJ, USA, 2014. IEEE Press.